Published in final edited form as:
Cell. 2013 April 25; 153(3): 521–534. doi:10.1016/j.cell.2013.03.022.

TNF Dually Mediates Resistance and Susceptibility to Mycobacteria Through Mitochondrial Reactive Oxygen Species

Francisco J. Roca[1] and **Lalita Ramakrishnan**[1,2,3]

[1]Departments of Microbiology, University of Washington Seattle, WA 98195, USA

[2]Departments of Medicine University of Washington Seattle, WA 98195, USA

[3]Departments of Immunology, University of Washington Seattle, WA 98195, USA

Summary

Tumor Necrosis Factor (TNF) constitutes a critical host defense against tuberculosis but its excess is also implicated in tuberculosis pathogenesis in zebrafish and humans. We elucidate the pathways by which TNF mediates tuberculosis pathogenesis using the zebrafish. TNF excess induces mitochondrial reactive oxygen species (ROS) in infected macrophages through RIP1–RIP3-dependent pathways. While initially increasing macrophage microbicidal activity, ROS rapidly induce programmed necrosis (necroptosis) and, release mycobacteria into the growth-permissive extracellular milieu. TNF-induced necroptosis occurs through two pathways: modulation of mitochondrial cyclophilin D, implicated in mitochondrial permeability transition pore formation, and acid sphingomyelinase-mediated ceramide production. Combined genetic blockade of cyclophilin D and acid sphingomyelinase renders the high TNF state hyperresistant by preventing macrophage necrosis while preserving increased microbicidal activity. Similarly, the cyclophilin D-inhibiting drug alisporivir and the acid sphingomyelinase-inactivating drug, desipramine, synergize to reverse susceptibility, suggesting the therapeutic potential of these orally-active drugs against tuberculosis and possibly other TNF-mediated diseases.

Introduction

While tuberculosis (TB) has traditionally been linked to failed immunity, recent work has implicated excessive inflammation in increased tuberculosis susceptibility (Agarwal et al., 2009; Berg and Ramakrishnan, 2012; Tobin et al., 2012). Studies in the zebrafish revealed that leukotriene A4 hydrolase (LTA4H) mediates susceptibility to *Mycobacterium marinum* (Mm) infection (Tobin et al., 2012; Tobin et al., 2010). LTA4H catalyzes the final step in the formation of the inflammatory lipid mediator leukotriene B4 (LTB_4), and LTA4H deficiency shunts eicosanoid production from LTB_4 to anti-inflammatory lipoxins that inhibit TNF production. LTA4H excess increases LTB_4, which induces TNF. Despite their opposite effects on TNF levels, LTA4H deficiency (LTA4H-low) and excess (LTA4H-high) states both produce susceptibility via necrosis of infected macrophages, allowing the release of mycobacteria into the growth-permissive extracellular milieu (Tobin et al., 2012). The TNF deficit in the LTA4H-low state reduces macrophage microbicidal activity, leading to increased intracellular bacterial growth followed by necrosis of the overladen macrophages (Tobin et al., 2010) (Figure 1). The high LTA4H/TNF state produces necrosis of infected macrophages despite their enhanced capacity to curtail bacterial growth (Figure 1).

In humans, a common single nucleotide polymorphism that regulates *LTA4H* expression was associated with TB meningitis severity (Tobin et al., 2012). Individuals homozygous for

Correspondence: lalitar@uw.edu.

the high expression and low expression alleles had similarly increased disease severity. Heterozygotes with an intermediate inflammatory state were the least susceptible. Of therapeutic importance, individuals with the low and high inflammatory states had divergent responses to adjunctive glucocorticoid treatment routinely given for TB meningitis. The survival benefit conferred by these potent anti-inflammatory drugs was confined to persons with the pro-inflammatory *LTA4H* genotype—with data suggesting that glucocorticoids might increase mortality in persons with the low-inflammatory *LTA4H* genotype.

Having established the importance of the high LTA4H/TNF state in human TB severity and treatment responsiveness, it was important to understand the mechanisms by which TNF excess produces susceptibility. Using the zebrafish, we interrogated the molecular pathways whereby high TNF promotes early macrophage resistance to mycobacteria only to be followed by macrophage lysis and extracellular bacterial proliferation. We show that excess TNF activates a programmed necrosis (necroptosis) pathway through mitochondrial ROS production. We have identified pharmacologic interventions in this pathway including alisporivir, a cyclophilin D inhibitor in phase III clinical trials for treatment of hepatitis C, and desipramine, a long-used tricyclic antidepressant that inactivates acid sphingomyelinase. Along with the identification of highly specific, genotype-directed therapies for TB, our findings may provide insights into the pathogenesis of, and therapeutic possibilities for, other inflammatory diseases that respond to TNF blockade.

Results

TNF excess triggers ROS production that kills both mycobacteria and infected macrophages

We searched for a common mechanism by excess TNF produced in the LTA4H-high state might kill intracellular bacteria and then the infected macrophages themselves. We considered previous findings that TNF-induced necrosis can occur through induction of ROS, which are powerful microbicidal agents (Schulze-Osthoff et al., 1992; Vandenabeele et al., 2010). Incubation of infected LTA4H-high fish, created by the injection of *lta4h* RNA (Tobin et al., 2012), with four different ROS scavengers (NAC, GSH, amifostine and TEMPOL) abolished both the initial macrophage microbicidal activity and the subsequent increase in whole fish bacterial burdens that result upon macrophage death (Figures 1, 2A-2C and Figure S1A-S1F). ROS scavengers did not render WT fish hypersusceptible, consistent with the literature reporting that Mm and *Mycobacterium tuberculosis* (Mtb) have multiple mechanisms to counter ROS to the extent that it is produced in WT infection (Figure 2A and 2B and Figure S1A-F) (Chan et al., 1992; Cirillo et al., 2009; Ehrt and Schnappinger, 2009; Subbian et al., 2007). Reactive nitrogen species (RNS) have been shown to work in conjunction with ROS to induce programmed necrosis under some conditions (Davis et al., 2010). However, they were not involved here. The nitric oxide (NO) scavenger c-PTIO had no effect on LTA4H-high bacterial burdens, while increasing those of WT animals consistent with the known mycobactericidal role of NO in mammalian systems (MacMicking et al., 1997) (Figure S2).

As TNF is the principal mediator of LTA4H-high susceptibility, ROS scavenging should also reverse the phenotypes of animals rendered into a high-TNF state by recombinant TNF injection (Tobin et al., 2012). As expected, NAC increased intramacrophage and overall bacterial burdens of 1 day post-infection (dpi) animals within 10 hours of co-administration with TNF (Figure 2D and data not shown); this effect was reversed 48 hours later (Figure 2E). Thus, TNF-induced ROS mediate their bactericidal effect within hours but this effect is soon nullified.

Our prior work showed that the secondary increase in bacterial burdens was associated with macrophage lysis (Tobin et al., 2012). In addition to macrophages, neutrophils can also become infected in the early granuloma and mediate oxidative bacterial killing (Yang et al., 2012). To determine if neutrophils were also being lysed by the increased ROS generated in the LTA4H-high/TNF-high state, we used a double transgenic line *Tg(mpeg1:YFP)/Tg(lyz:DsRED2)* with yellow fluorescent macrophages and red fluorescent neutrophils. As expected, macrophages were reduced at 2 dpi, when the early reduction of bacterial burdens is first nullified and extracellular bacteria are first discernible (Figure 2F and 2G, and data not shown). However, neutrophil numbers were unchanged (Figure 2F). We found no reduction in macrophage numbers in uninfected LTA4H/TNF-high animals both by assessing *mpeg1:YFP*-positive cells and cells staining with neutral red, a macrophage-specific vital stain (Yang et al., 2012) (Figure 2H and Figure S3A). Thus, the high TNF state does not lead to a baseline reduction in macrophage development or survival; rather macrophages are depleted only upon infection. Finally, we confirmed that the ROS scavenger NAC reversed the macrophage lysis and the ensuing bacterial cording, a reliable indicator of the presence of extracellular bacteria, of TNF-high animals (Figure 2F, 2I and 2J and Figure S3B).

To verify independently that TNF-high susceptibility was mediated via excess ROS, we quantified ROS production in live animals using the cell-permeant ROS indicator CM-H_2DCFDA, which fluoresces green upon oxidation. Fluorescence microscopy at 1 dpi revealed only infected TNF-high to have bright green fluorescent (ROS-positive) cells, whereas neither infected WT nor TNF-high uninfected animals did. The ROS-positive cells were invariably infected, further suggesting that only infected macrophages produce ROS (Figure 2K). Whole animal quantitation of ROS production by fluorimetry confirmed ROS to increase only in infected TNF-high fish, suggesting that TNF excess and infection must act in concert to increase ROS production (Figure 2L). NAC abolished this ROS production, corroborating that it reduces susceptibility in high TNF animal specifically through its ROS scavenging activity (Figure 2M). Finally we showed that the increased ROS is macrophage-dependent by selectively knocking down macrophages using a PU.1 morpholino (Clay et al., 2007; He et al., 2012; Su et al., 2007). Macrophage depletion of TNF-high fish returned ROS levels to WT despite having similar bacterial burdens at the time of assessment (Figure 2N and data not shown).

Collectively, these experiments reveal that TNF excess increases ROS production in infected macrophages. This increase is initially bactericidal, but rapidly becomes host-detrimental by lysing the infected macrophages and placing mycobacteria in a permissive extracellular milieu.

TNF excess mediates necrosis through the RIP1-RIP3 kinase pathway

TNF can mediate apoptosis and programmed necrosis, both of which are found in TB and have been associated with ROS production (Fiers et al., 1999; Laster et al., 1988; Ramakrishnan, 2012). We ruled out that high TNF-mediated cell death was occurring through apoptosis by showing that the pancaspase inhibitor Q-VD-OPh, which reduces TUNEL-positive macrophages in zebrafish larval granulomas by ~ 90% (Yang et al., 2012) did not rescue LTA4H/TNF-high hypersusceptibility (Figure S4). TNF-mediated programmed necrosis typically involves the receptor-interacting serine-threonine kinases 1 and 3 (RIP1 and RIP3), as evidenced in human, mouse, and zebrafish cell lines, as well as in a murine sepsis model (Cho et al., 2009; He et al., 2009; Holler et al., 2000; Zhang et al., 2009). Zebrafish orthologs of human RIP1 and RIP3 are similarly organized with strong conservation of all functional domains (Myers and Miller, 1988; Vandenabeele et al., 2010) (Figure 3A). To initiate necrosis, the TNF-TNF-R complex typically first recruits RIP1 via death domain interactions. RIP3 then binds to RIP1 via their RHIM domains. RIP1-RIP3

binding initiates RIP3 phosphorylation, which in turn activates other members of the so-called necroptosome complex. RIP1 and RIP3 mopholino knockdown reversed both of the phenotypes associated with the LTA4H-high state: early macrophage microbicidal activity and the subsequent increased bacterial burdens associated with bacterial cording (Figure 3B-3G). We confirmed that they similarly reversed TNF-high phenotypes as well (Figure 3H-3J). The mammalian RIP1 inhibitors, necrostatin-1 and necrostatin-5 also reversed the LTA4H-high phenotypes (Figure 3K-3M and Figure S5A-S3C) (Degterev et al., 2008). RIP1 and RIP3 knockdown did not alter the bacterial burden of WT and LTA4H-low animals, showing that this programmed necrosis pathway operates only under LTA4H/TNF-high conditions in the context of mycobacterial infection (Figure S3D-S5H).

The TNF-RIP1-RIP3 axis mediates necrosis of infected macrophages through mitochondrial ROS production

The mitochondrion is a major source of cellular ROS, and mitochondrial ROS are implicated in the pathogenesis of a variety of diseases (Nunnari and Suomalainen, 2012; Orrenius et al., 2007). While apoptotic cell death has long been linked to the mitochondrion, recent literature reports the role of the mitochondrion in programmed necrosis with the identification of RIP3 substrates essential for this process (Sun et al., 2012; Wang et al., 2012; Zhang et al., 2009). To determine if the TNF-mediated necrosis occurring in Mm infection involves the mitochondrion, we took two experimental approaches. First, we asked if the susceptibility phenotypes would be abrogated by Necrox-5, a new ROS scavenger that localizes mainly to the mitochondrion and inhibits TNF/RIP1-3-dependent necroptosis in different mammalian systems (Kim et al., 2010a). Necrox-5 reversed the late increase in bacterial burdens and cording of both LTA4H-high and TNF-high animals without altering bacterial burdens in WT and LTA4H-low animals, suggesting a specific role for mitochondrial ROS in TNF-mediated susceptibility (Figure 4A-4D, and data not shown).

Next, we assessed the impact of the recently discovered RIP3 substrates MLKL and PGAM5, which link programmed necrosis to the mitochondrion (Sun et al., 2012; Wang et al., 2012; Zhang et al., 2009). RIP3 binds and phosphorylates MLKL and this complex then serves as a platform for the binding and activation of the mitochondrial phosphatase PGAM5. Activated PGAM5 dephosphorylates Drp1, enabling it to form homodimers required for mitochondrial fission and fusion (Sun et al., 2012; Wang et al., 2012; Zhang et al., 2009). By promoting processes closely linked to mitochondrial turnover, Drp1 has also been shown to trigger ROS production and cell death (Suen et al., 2008). We could not identify the zebrafish ortholog for MLKL for morpholino knockdown. So we used the small molecule called necrosulfonamide, which binds human MLKL and sterically hinders its binding to RIP3 (Sun et al., 2012). Necrosulfonamide specifically reversed LTA4H-high hypersusceptiblity (Figure 4E). Similarly, a PGAM5 morpholino knockdown reversed all LTA4H-high susceptibility phenotypes (Figure 4F-4H)

These experiments provided genetic evidence for mitochondrial involvement in LTA4H/TNF-high macrophage lysis and susceptibility. We next sought to visualize directly this sequence of events. Infected larvae were injected with TNF or vehicle for two hours, after which they were injected with MitoTracker Red CM-H_2Xros, a redox-sensitive dye that targets the mitochondrion and fluoresces red upon oxidation (Kweon et al., 2001) and SYTOX green, a cell membrane impermeable nucleic acid stain. With this combination, only mitochondrial ROS production should render cells red fluorescent and only cells with compromised cell membranes should become green fluorescent. We predicted that 1) red fluorescent macrophages will be found only after TNF administration and will comprise mostly of infected cells, and 2) Red fluorescence will precede green fluorescence, the appearance of which will be associated with a lost of cellular integrity. Serial imaging of 40 infected animals over 7 hours following TNF administration confirmed these predictions.

Red fluorescence first appeared 3 hours after TNF administration and was restricted to infected macrophages (Figure 4I). No red fluorescence was observed in vehicle-treated animals. Green fluorescence appeared after an additional two hours, and only in red fluorescent cells (Figure 4J and 4K). Its appearance was associated with the progressive loss of membrane integrity on bright-field imaging (Figure 4I-K). These serial microscopical observations corroborate the genetic data that TNF induces programed necrosis of *Mycobacterium*-infected macrophages through mitochondrial ROS production.

Finally, we asked if TNF activation of phagosomal oxidase NOX2 ($gp91^{phox}$) contributed to our phenotypes because of the following connections in the literature: in phagocytes, TNF is a potent NOX2 activator (Dewas et al., 2003), and in fibroblasts, TNF- RIP-1 activation of NOX1 (non-phagocytic NOX2 isoform)-derived ROS induces necrosis (Kim et al., 2007), and NOX1 activation is required to sustain ROS production initiated in the mitochondrion so as to promote cell death (Lee et al., 2006b). However, we found that in LTA4H-high animals, morpholino $gp91^{phox}$ knockdown reversed neither early resistance nor later susceptibility (Figure S6A and S6B). Morpholino efficacy was confirmed by showing that $gp91^{phox}$ morphants had the expected susceptibility to *Pseudomonas aeruginosa* (Figure S6C)(Yang et al., 2012). In sum, our data suggest a direct and sole TNF-mediated induction of mitochondrial ROS during infection.

Cyclophilin D regulates the mitochondrial permeability transition pore complex to induce TNF-mediated necrosis

How do mitochondrial ROS trigger cell necrosis? Prior findings suggested this may occur via formation of the mitochondrial permeability transition pore complex (mPTPC), a crucial step in mitochondrial demolition (Figure S7) (Baines et al., 2005; Crompton et al., 1988; Nakagawa et al., 2005). The mitochondrial matrix protein cyclophilin D (CYPD) has been shown to be a critical regulator of mPTPC activity in response to oxidative or calcium stress (Figure S7) (Vandenabeele et al., 2010). CYPD morpholino knockdown reversed the high bacterial burdens of LTA4H-high fish, suggesting mPTPC involvement (Figure 5A). Given that this intervention is downstream of TNF-mediated ROS production, our model predicts that CYPD knockdown should preserve the early increased macrophage microbicidal activity that is reversed by interventions upstream of ROS production. We found this to be the case (Figure 5B – compare to Figures 3B, 3E, 3H and 3K, and 4F where macrophage microbicidal activity was measured in the context of RIP1, RIP3 and PGAM5). ROS quantification in the corresponding morphants further confirms the model – RIP1, RIP3 and PGAM5 knockdown reduced ROS of TNF-high fish down to WT levels. In contrast, ROS levels were higher in TNF-high CYPD morphants, likely due to continued production by intact infected macrophages (Figure 5C).

Collectively these data implicate CYPD and the mPTPC in the pathogenesis of TNF-mediated necrosis. However a closer examination of the data raises a conundrum: given the retention of increased macrophage microbicidal activity in the TNF-high CYPD morphants, why are their later bacterial burdens not lowered significantly below those of WT fish (Figure 5A)? Could an additional pathway of TNF-mediated cell necrosis be masking such a hyperresistance phenotype? An analysis of macrophage loss in the TNF-high CYPD morphants supported this possibility: macrophage numbers were not restored in these morphants in contrast to those in TNF-high RIP1 morphants where ROS overproduction is abolished (Figure 5D).

Acid sphingomyelinase-mediated ceramide production contributes to cell necrosis in the TNF-high state

One additional pathway of TNF-mediated necrosis occurs through activation of sphingomyelinases that results in the production of ceramide, an inducer of both apoptosis and RIP1-dependent programmed necrosis (Thon et al., 2005; Vandenabeele et al., 2010). Lysosomal acid sphingomyelinase (aSMase) can also be activated by oxidation (Dumitru and Gulbins, 2006), making it a promising candidate mediator of the residual cell necrosis in the TNF-high animals. aSMase morpholino knockdown revealed the substantial contribution of this pathway: aSMase morphants phenocopied CYPD morphants under high-TNF conditions, preserving increased macrophage microbicidal activity while reversing later bacterial burdens to WT levels but not below (Figure 5E and 5F). That this phenotype was due to ceramide reduction was shown by reproducing it with acid ceramidase overexpression (Figure 5E and 5F).

If these two pathways together are wholly responsible for TNF-mediated necrosis, then knocking them down together should prevent necrosis completely, allowing the increased microbicidal capacity of macrophages to then confer hyperresistance. Assessment of macrophage survival and bacterial burdens in single and double knockdowns of the two pathways showed this to be the case. The residual levels of cell necrosis in the single knockdowns were completely eliminated in the double knockdowns (Figure 5G). Accordingly, these animals were now hyperresistant to infection, with bacterial burdens being reduced below WT levels even at later stages of infection (Figure 5H). NAC treatment reverted the bacterial loads of these animals to WT levels, confirming their hyperresistance to be due to increased ROS production (Figure 5I). Together, these experiments suggest that preventing death of ROS-producing macrophages can prolong microbicidal activity and substantially reduce bacterial burdens over WT.

Pharmacological interventions in the TNF-mediated necrosis pathway as host-targeting antitubercular drugs

There is currently substantial interest in pharmacologic manipulation of programmed necrosis pathways in a variety of inflammatory diseases (Galluzzi et al., 2011; Vandenabeele et al., 2010). In the course of elucidating the high TNF-mediated pathway, we used small molecules, several of which are approved drugs (NAC, amifostine), drugs in clinical trials (TEMPOL), or over the counter supplements (reduced glutathione) (Table S2). These agents all act upstream of ROS production thus reverting intramacrophage bacterial burdens and later bacterial burdens to WT levels but no lower (e.g. Figure 2A and 2B). With our discovery that genetic interventions downstream of ROS have the potential to convert TNF-mediated hypersusceptibility to a hyperresistant state, we searched for drugs that could inhibit these pathways.

We identified two candidates. The first, alisporivir (Debio 025), is an orally administered drug that impedes CYPD's ability to regulate mPTPC and is currently in Phase III clinical development for Hepatitis C (Quarato et al., 2012; Tiepolo et al., 2009). As with the CYPD morpholino, alisporivir (10 μM) reversed the susceptibility of LTA4H-high animals to WT levels while retaining the early improved microbicidal activity (Figure 6A and 6B). Like the CYPD morpholino, alisporivir's failure to confer hyperresistance could be explained by residual macrophage necrosis (Figure 6C). These results suggested that it was acting specifically on CYPD, substantiated further by its failure to alter bacterial burdens either in WT or LTA4H-low animals (Figure 6A and 6D).

Second, we tested the tricyclic class of antidepressants, known to promote specific proteolytic degradation of aSMase and thereby expected to reduce cell death through

inhibiting ceramide production (Elojeimy et al., 2006). As predicted by our model, desipramine, a tricyclic antidepressant in clinical use for nearly 50 years, produced susceptibility specifically of LTA4H-high but not WT animals (Figure 6E). Toxicity of alisporivir and desipramine at their effective doses of 10 and 7.5 μM respectively, precluded using this dose combination to test for their predicted synergy. Instead, we asked if subtherapeutic concentrations of each drug (7.5 μM of alisporivir and 5 μM of desipramine) would be effective in combination (Takaki et al., 2012). We found that they were: combination therapy significantly reduced bacterial burdens of TNF-high fish and trended towards making the fish hyperresistant, as predicted (Figure 6F).

As a final demonstration of the specificity of the two drugs, we tested their effects in aSMAse and CYPD morphants. If each drug is specific to its pathway, then alisporivir but not desipramine should further reduce the bacterial burdens of the aSMase morphants. Conversely, desipramine but not alisporivir should further reduce the bacterial burdens of the CYPD morphants. Exactly this was observed, confirming the specificity of action of the two drugs (Figure 6G and 6H).

Discussion

Using the zebrafish, we have identified a potential mechanism to account for the worse outcomes in TB meningitis patients with pro-inflammatory *LTA4H* genotypes (Tobin et al., 2012) (Figure 7 and Table S3). This mechanism may account for outcomes in other forms of TB as well. Our findings explain the previously observed dichotomy of the LTA4H-high zebrafish phenotypes: an initial enhancement of macrophage microbicidal activity followed by increased bacterial burden. We identify mitochondrial ROS as critical mediators of both phenotypes: the latter is accomplished by triggering cell lysis, thus not only terminating beneficial ROS production but also releasing the bacteria into the permissive extracellular milieu. ROS-dependent cell necrosis is mediated by at least two pathways that each participates substantially in cell death. Blocking either reverts bacterial burdens to WT levels; blocking both converts the hypersusceptible state to a hyperresistant one.

This understanding leads to potential therapeutic interventions. Several of the ROS scavengers we tested are being used or tested as drugs. Even more exciting is our identification of two oral drugs, alisporivir and desipramine, that work both singly and synergistically to block ROS-mediated cell necrosis (Figure 7). Interventions in this pathway are beneficial only to the genotypes with increased ROS production, but do not adversely affect those where the high TNF pathway is not operant. This is in contrast to more upstream interventions, e.g. glucocorticoids in which only one of the two genotypes - LTA4H-high or LTA4H-low - benefitted while the other was harmed (Tobin et al., 2012).

TNF-mediated RIP1/RIP3-dependent cell necrosis appears to be a mechanism for control of replication of viral pathogens via cellular niche destruction (Vandenabeele et al., 2010). Like other pro-inflammatory mechanisms, this mechanism is also implicated in the pathology of a growing list of inflammatory diseases including sepsis (Duprez et al., 2011; Galluzzi et al., 2011). The lifestyle of the pathogenic mycobacteria makes them adept at exploiting this host-mediated necrosis: while using macrophages for systemic invasion of the host and dissemination therein, they later benefit from becoming extracellular so as to increase their numbers and their transmissibility (Clay et al., 2007; Davis and Ramakrishnan, 2009; Ramakrishnan, 2012). Indeed, our data suggest that excess TNF is necessary but not sufficient for macrophage necrosis. The bacterium plays a critical role in TNF-mediated ROS production, using yet unknown determinants. These might not represent classical virulence determinants but ones that only mediate virulence in the context of certain host inflammatory profiles. Mycobacteria are already known to induce host lipoxin production that can induce a non-programmed cell necrosis by inhibiting TNF production (Cassidy-

Stone et al., 2008; Tobin et al., 2010). This work now implicates mycobacterial factors in programmed necrosis as well. Several other intracellular pathogens have been shown to induce caspase-1-dependent phagocyte lysis but this appears to be host-beneficial (Bergsbaken et al., 2009). Recently, *Salmonella* was also found to mediate a pathogen-beneficial RIP-1-mediated cell necrosis (Robinson et al., 2012). While that study implicated Type 1 interferons, we speculate that downstream events such as ROS production and mPTPC formation may be shared with the pathway we have uncovered, revealing common treatment modalities for other infections.

Our data reveal ROS as both susceptibility and resistance factors in TB, involving a complex interplay between host and pathogen. Mycobacteria have evolved to counter ROS both by inhibiting their production, and by detoxifying them (Ehrt and Schnappinger, 2009). Despite these bacterial mechanisms, ROS production appears to have at least a modest effect in restraining mycobacteria, as shown by recent work in the zebrafish suggesting that neutrophils can kill phagocytosed mycobacteria through oxidative mechanisms (Yang et al., 2012). This may be because the higher levels of ROS produced by neutrophils are not effectively countered by mycobacterial mechanisms. Our current work indicates that ROS overproduction in macrophages is also not countered by mycobacteria; however it is host-detrimental rather than host protective. Moreover, our finding that macrophage ROS production is mitochondrial and dependent on a bacterial component is intriguing in light of reports that specific mycobacterial determinants target the host mitochondrion to produce cell death (Cadieux et al., 2011; Sohn et al., 2011). Such mycobacterial-mitochondrial interactions may potentiate ROS overproduction in the context of host-driven pathways.

Our discovery of the role of ceramide in cell necrosis links data implicating these host lipids in TNF-mediated necrosis to host lipidomic and proteomic analyses showing that aSMAse activity is increased during Mtb infection (Lee et al., 2006a; Lee et al., 2011). Mtb infection in cultured macrophages can lead to lysosome-dependent infected cell necrosis by promoting lysosomal membrane permeabilization, release of lysosomal enzymes and lipase activation, which promotes mitochondrial disruption (Lee et al., 2011). However, this mode of cell death is driven by high intracellular bacterial load and is mPTPC-independent. While we cannot tell if ceramide production in our system acts through the mitochondrion or not, we do know that it occurs in the context of high-TNF infection even when bacterial burdens are very low. Ceramide production may be triggered by bacterially-induced ROS. Furthermore, precisely how ceramide works to lyse macrophages is unknown; it could be acting on the mitochondrion to potentiate CYPD-mediated mPTPC or elsewhere in the cell (Thon et al., 2005). Regardless of mechanism, this pathway may be important in advanced human TB, where ceramide is increased in necrotic lung granulomas (Kim et al., 2010b).

While our findings suggest the potential for dual blockade of the CYPD and ceramide-mediated necrosis pathways to produce hyperresistance, they must be interpreted with caution. Increased ROS production is likely to eventually kill the cell even with both of these pathways blocked - through lipid peroxidation, DNA damage, activation of pro-apoptotic factors and ATP depletion (Vandenabeele et al., 2010). Hence the delay in cell death by blocking these two pathways would be most useful if it is long enough to allow macrophage ROS to eradicate the bacteria. Macrophage sterilization may be potentiated by combining necrosis-blocking drugs with traditional antitubercular drugs.

Furthermore, we have not directly shown high TNF to be the culprit in human high-LTA4H-mediated TB susceptibility, only increased inflammation that may involve different mediators. Our zebrafish findings, however have been previously validated in humans. It is additionally reassuring that the disease-promoting pathway we described is amenable to rationally designed interventions using chemicals and drugs identified in human systems

(Figure 7). Our finding that necrosulfonamide is effective makes a particularly strong case for the zebrafish; this chemical discovered using a human cell line was found to be ineffective in a murine system because it prevents MLKL-RIP3 interaction by steric hindrance through binding to a nonessential cysteine residue that is present in humans but not mice (Wang et al., 2012). While a clear zebrafish homolog is yet to be annotated, we have identified a homologous domain corresponding to 42 amino acid residues of the human protein within the functional sequence (protein kinase domain), in which the cysteine residue is conserved [Chromosome 12, nucleotide sequence from 15174549 to 15174674, identities = 16/47 (34%), positives = 27/47 (57%)]. Finally, two clinical studies point to the potential importance of this pathway in humans. First, the high-expressing LTA4H allele is relatively rare in Africa ((Stranger et al., 2007) and our unpublished data), yet glucocorticoids have been shown to have similar, small beneficial effects in TB meningitis in African and Vietnamese populations (Schoeman et al., 1997; Thwaites et al., 2004), suggesting that a hyper-inflammatory state in TB may arise via alternative mechanisms, perhaps through genetic variation in other components of the pathway detailed in this investigation. Second, that these susceptibility pathways could be TNF-mediated is supported by a clinical trial from Uganda showing that pulmonary TB patients had increased clearance of sputum bacteria when treated with TNF blocking agents (Wallis, 2005).

In summary, variants in multiple human loci involving our newly discovered pathway may alter host response to mycobacterial infection. Given the druggability of this pathway, their identification in human prospective studies is promising. Finally, TNF-mediated ROS production may play a similar role in the pathogenesis of other diseases where TNF is known to play a pathogenic role, such as rheumatoid arthritis, ankylosing spondylitis, sarcoidosis, Crohn's disease and granulomatosis with polyangiitis (Keystone and Ware, 2010) in which ROS scavengers, alisporivir and the tricyclic antidepressants may be effective.

Experimental Procedures

Bacterial Strains

WT Mm (strain M - ATCC #BAA-535) or the Mm *erp* mutant (Cosma et al., 2006) constitutively expressing tdTomato (red fluorescence), and Mm expressing tdKatushka2 (far-red fluorescence), or EBFP2 (blue fluorescence) were used for fluorescence microscopy and quantitation of intracellular bacterial burdens. *erp* mutant Mm was used to enumerate intracellular bacteria and WT Mm was used for all other assays as detailed in Supplementary Experimental Procedures.

Zebrafish infection

Zebrafish experiments were conducted in conformity with the Public Health Service Policy on Humane Care and Use of Laboratory Animals using protocols approved by the Institutional Animal Care and Use Committee of the University of Washington. 90-150 Mm was injected into the caudal vein of 36-48 hpf larvae of the AB line and the *Tg(mpeg1:YFP)* line created from it as detailed in Supplementary Experimental Procedures.

ROS detection and quantification assay

ROS accumulation was assessed by the levels of the oxidized form of the cell-permeant ROS indicator acetyl ester of 5-(and 6-) chloromethyl-2′,7′-dichlorodihydrofluorescein diacetate (CM-H_2DCFDA) (Invitrogen), as detailed in Supplementary Experimental Procedures.

Mitochondrial ROS and cell death detection assays

Mitochondrial ROS production and cell death was assayed by the levels of the oxidized form of the cell permeant mitochondrion-targeted ROS indicator, MitoTracker Red CM-H_2Xros and the live cell impermeant nucleic acid stain SYTOX Green (both from Invitrogen) as detailed in Supplementary Experimental Procedures.

Supplementary Material

Refer to Web version on PubMed Central for supplementary material.

Acknowledgments

We thank X. Lei and Novartis Inc. for the gifts of necrosulfonamide and alisporivir, C.-T. Yang for the *Tg(mpeg1:YFP)* zebrafish line, A. Oberst and D. Tobin for advice and discussion, C. Cosma for advice on statistical analysis, and A. Pagán, J. Szumowski, C. Cosma, A. Oberst, D. Tobin and K. Takaki for manuscript review, and J. Cameron for fish facility management. Funded by grants from the NIH and the NWRCE for Biodefense and Emerging Infectious Diseases Research (L.R.), and a postdoctoral fellowship from the educational ministry of Spain (F.J.R). L.R. is a recipient of the NIH Director's Pioneer Award.

References

Agarwal N, Lamichhane G, Gupta R, Nolan S, Bishai WR. Cyclic AMP intoxication of macrophages by a Mycobacterium tuberculosis adenylate cyclase. Nature. 2009; 460:98–102. [PubMed: 19516256]

Baines CP, Kaiser RA, Purcell NH, Blair NS, Osinska H, Hambleton MA, Brunskill EW, Sayen MR, Gottlieb RA, Dorn GW, et al. Loss of cyclophilin D reveals a critical role for mitochondrial permeability transition in cell death. Nature. 2005; 434:658–662. [PubMed: 15800627]

Berg RD, Ramakrishnan L. Insights into tuberculosis from the zebrafish model. Trends Mol Med. 2012

Bergsbaken T, Fink SL, Cookson BT. Pyroptosis: host cell death and inflammation. Nat Rev Microbiol. 2009; 7:99–109. [PubMed: 19148178]

Cadieux N, Parra M, Cohen H, Maric D, Morris SL, Brennan MJ. Induction of cell death after localization to the host cell mitochondria by the Mycobacterium tuberculosis PE_PGRS33 protein. Microbiology. 2011; 157:793–804. [PubMed: 21081760]

Cassidy-Stone A, Chipuk JE, Ingerman E, Song C, Yoo C, Kuwana T, Kurth MJ, Shaw JT, Hinshaw JE, Green DR, et al. Chemical inhibition of the mitochondrial division dynamin reveals its role in Bax/Bak-dependent mitochondrial outer membrane permeabilization. Dev Cell. 2008; 14:193–204. [PubMed: 18267088]

Chan J, Xing Y, Magliozzo RS, Bloom BR. Killing of virulent Mycobacterium tuberculosis by reactive nitrogen intermediates produced by activated murine macrophages. J Exp Med. 1992; 175:1111–1122. [PubMed: 1552282]

Cho YS, Challa S, Moquin D, Genga R, Ray TD, Guildford M, Chan FK. Phosphorylation-driven assembly of the RIP1-RIP3 complex regulates programmed necrosis and virus-induced inflammation. Cell. 2009; 137:1112–1123. [PubMed: 19524513]

Cirillo SL, Subbian S, Chen B, Weisbrod TR, Jacobs WR Jr, Cirillo JD. Protection of Mycobacterium tuberculosis from reactive oxygen species conferred by the mel2 locus impacts persistence and dissemination. Infect Immun. 2009; 77:2557–2567. [PubMed: 19349422]

Clay H, Davis J, Beery D, Huttenlocher A, Lyons S, Ramakrishnan L. Dichotomous Role of the Macrophage in Early Mycobacterium marinum Infection of the Zebrafish. Cell Host and Microbe. 2007; 2:29–39. [PubMed: 18005715]

Crompton M, Ellinger H, Costi A. Inhibition by cyclosporin A of a Ca2+-dependent pore in heart mitochondria activated by inorganic phosphate and oxidative stress. Biochem J. 1988; 255:357–360. [PubMed: 3196322]

Davis CW, Hawkins BJ, Ramasamy S, Irrinki KM, Cameron BA, Islam K, Daswani VP, Doonan PJ, Manevich Y, Madesh M. Nitration of the mitochondrial complex I subunit NDUFB8 elicits RIP1- and RIP3-mediated necrosis. Free Radic Biol Med. 2010; 48:306–317. [PubMed: 19897030]

Davis JM, Ramakrishnan L. The role of the granuloma in expansion and dissemination of early tuberculous infection. Cell. 2009; 136:37–49. [PubMed: 19135887]

Degterev A, Hitomi J, Germscheid M, Ch'en IL, Korkina O, Teng X, Abbott D, Cuny GD, Yuan C, Wagner G, et al. Identification of RIP1 kinase as a specific cellular target of necrostatins. Nat Chem Biol. 2008; 4:313–321. [PubMed: 18408713]

Dewas C, Dang PM, Gougerot-Pocidalo MA, El-Benna J. TNF-alpha induces phosphorylation of p47(phox) in human neutrophils: partial phosphorylation of p47phox is a common event of priming of human neutrophils by TNF-alpha and granulocyte-macrophage colony-stimulating factor. J Immunol. 2003; 171:4392–4398. [PubMed: 14530365]

Dumitru CA, Gulbins E. TRAIL activates acid sphingomyelinase via a redox mechanism and releases ceramide to trigger apoptosis. Oncogene. 2006; 25:5612–5625. [PubMed: 16636669]

Duprez L, Takahashi N, Van Hauwermeiren F, Vandendriessche B, Goossens V, Vanden Berghe T, Declercq W, Libert C, Cauwels A, Vandenabeele P. RIP kinase-dependent necrosis drives lethal systemic inflammatory response syndrome. Immunity. 2011; 35:908–918. [PubMed: 22195746]

Ehrt S, Schnappinger D. Mycobacterial survival strategies in the phagosome: defence against host stresses. Cell Microbiol. 2009; 11:1170–1178. [PubMed: 19438516]

Elojeimy S, Holman DH, Liu X, El-Zawahry A, Villani M, Cheng JC, Mahdy A, Zeidan Y, Bielwaska A, Hannun YA, et al. New insights on the use of desipramine as an inhibitor for acid ceramidase. FEBS Lett. 2006; 580:4751–4756. [PubMed: 16901483]

Fiers W, Beyaert R, Declercq W, Vandenabeele P. More than one way to die: apoptosis, necrosis and reactive oxygen damage. Oncogene. 1999; 18:7719–7730. [PubMed: 10618712]

Galluzzi L, Vanden Berghe T, Vanlangenakker N, Buettner S, Eisenberg T, Vandenabeele P, Madeo F, Kroemer G. Programmed necrosis from molecules to health and disease. Int Rev Cell Mol Biol. 2011; 289:1–35. [PubMed: 21749897]

He S, Lamers GE, Beenakker JW, Cui C, Ghotra VP, Danen EH, Meijer AH, Spaink HP, Snaar-Jagalska BE. Neutrophil-mediated experimental metastasis is enhanced by VEGFR inhibition in a zebrafish xenograft model. J Pathol. 2012; 227:431–445. [PubMed: 22374800]

He S, Wang L, Miao L, Wang T, Du F, Zhao L, Wang X. Receptor interacting protein kinase-3 determines cellular necrotic response to TNF-alpha. Cell. 2009; 137:1100–1111. [PubMed: 19524512]

Holler N, Zaru R, Micheau O, Thome M, Attinger A, Valitutti S, Bodmer JL, Schneider P, Seed B, Tschopp J. Fas triggers an alternative, caspase-8-independent cell death pathway using the kinase RIP as effector molecule. Nat Immunol. 2000; 1:489–495. [PubMed: 11101870]

Keystone EC, Ware CF. Tumor necrosis factor and anti-tumor necrosis factor therapies. J Rheumatol Suppl. 2010; 85:27–39. [PubMed: 20436163]

Kim HJ, Koo SY, Ahn BH, Park O, Park DH, Seo DO, Won JH, Yim HJ, Kwak HS, Park HS, et al. NecroX as a novel class of mitochondrial reactive oxygen species and ONOO(-) scavenger. Arch Pharm Res. 2010a; 33:1813–1823. [PubMed: 21116785]

Kim MJ, Wainwright HC, Locketz M, Bekker LG, Walther GB, Dittrich C, Visser A, Wang W, Hsu FF, Wiehart U, et al. Caseation of human tuberculosis granulomas correlates with elevated host lipid metabolism. EMBO Mol Med. 2010b; 2:258–274. [PubMed: 20597103]

Kim YS, Morgan MJ, Choksi S, Liu ZG. TNF-induced activation of the Nox1 NADPH oxidase and its role in the induction of necrotic cell death. Mol Cell. 2007; 26:675–687. [PubMed: 17560373]

Kweon SM, Kim HJ, Lee ZW, Kim SJ, Kim SI, Paik SG, Ha KS. Realtime measurement of intracellular reactive oxygen species using Mito tracker orange (CMH2TMRos). Biosci Rep. 2001; 21:341–352. [PubMed: 11893000]

Laster SM, Wood JG, Gooding LR. Tumor necrosis factor can induce both apoptic and necrotic forms of cell lysis. J Immunol. 1988; 141:2629–2634. [PubMed: 3171180]

Lee J, Remold HG, Ieong MH, Kornfeld H. Macrophage apoptosis in response to high intracellular burden of Mycobacterium tuberculosis is mediated by a novel caspase-independent pathway. J Immunol. 2006a; 176:4267–4274. [PubMed: 16547264]

Lee J, Repasy T, Papavinasasundaram K, Sassetti C, Kornfeld H. Mycobacterium tuberculosis induces an atypical cell death mode to escape from infected macrophages. PLoS One. 2011; 6:e18367. [PubMed: 21483832]

Lee SB, Bae IH, Bae YS, Um HD. Link between mitochondria and NADPH oxidase 1 isozyme for the sustained production of reactive oxygen species and cell death. J Biol Chem. 2006b; 281:36228–36235. [PubMed: 17015444]

MacMicking JD, North RJ, LaCourse R, Mudgett JS, Shah SK, Nathan CF. Identification of nitric oxide synthase as a protective locus against tuberculosis. Proc Natl Acad Sci U S A. 1997; 94:5243–5248. [PubMed: 9144222]

Myers EW, Miller W. Optimal alignments in linear space. Comput Appl Biosci. 1988; 4:11–17. [PubMed: 3382986]

Nakagawa T, Shimizu S, Watanabe T, Yamaguchi O, Otsu K, Yamagata H, Inohara H, Kubo T, Tsujimoto Y. Cyclophilin D-dependent mitochondrial permeability transition regulates some necrotic but not apoptotic cell death. Nature. 2005; 434:652–658. [PubMed: 15800626]

Nunnari J, Suomalainen A. Mitochondria: in sickness and in health. Cell. 2012; 148:1145–1159. [PubMed: 22424226]

Orrenius S, Gogvadze V, Zhivotovsky B. Mitochondrial oxidative stress: implications for cell death. Annu Rev Pharmacol Toxicol. 2007; 47:143–183. [PubMed: 17029566]

Quarato G, D'Aprile A, Gavillet B, Vuagniaux G, Moradpour D, Capitanio N, Piccoli C. The cyclophilin inhibitor alisporivir prevents hepatitis C virus-mediated mitochondrial dysfunction. Hepatology. 2012; 55:1333–1343. [PubMed: 22135208]

Ramakrishnan L. Revisiting the role of the granuloma in tuberculosis. Nat Rev Immunol. 2012; 12:352–366. [PubMed: 22517424]

Robinson N, McComb S, Mulligan R, Dudani R, Krishnan L, Sad S. Type I interferon induces necroptosis in macrophages during infection with Salmonella enterica serovar Typhimurium. Nat Immunol. 2012; 13:954–962. [PubMed: 22922364]

Schoeman JF, Van Zyl LE, Laubscher JA, Donald PR. Effect of corticosteroids on intracranial pressure, computed tomographic findings, and clinical outcome in young children with tuberculous meningitis. Pediatrics. 1997; 99:226–231. [PubMed: 9024451]

Schulze-Osthoff K, Bakker AC, Vanhaesebroeck B, Beyaert R, Jacob WA, Fiers W. Cytotoxic activity of tumor necrosis factor is mediated by early damage of mitochondrial functions. Evidence for the involvement of mitochondrial radical generation. J Biol Chem. 1992; 267:5317–5323. [PubMed: 1312087]

Sohn H, Kim JS, Shin SJ, Kim K, Won CJ, Kim WS, Min KN, Choi HG, Lee JC, Park JK, et al. Targeting of Mycobacterium tuberculosis heparin-binding hemagglutinin to mitochondria in macrophages. PLoS Pathog. 2011; 7:e1002435. [PubMed: 22174691]

Stranger BE, Nica AC, Forrest MS, Dimas A, Bird CP, Beazley C, Ingle CE, Dunning M, Flicek P, Koller D, et al. Population genomics of human gene expression. Nat Genet. 2007; 39:1217–1224. [PubMed: 17873874]

Su F, Juarez MA, Cooke CL, Lapointe L, Shavit JA, Yamaoka JS, Lyons SE. Differential regulation of primitive myelopoiesis in the zebrafish by Spi-1/Pu.1 and C/ebp1. Zebrafish. 2007; 4:187–199. [PubMed: 18041923]

Subbian S, Mehta PK, Cirillo SL, Cirillo JD. The Mycobacterium marinum mel2 locus displays similarity to bacterial bioluminescence systems and plays a role in defense against reactive oxygen and nitrogen species. BMC Microbiol. 2007; 7:4. [PubMed: 17239244]

Suen DF, Norris KL, Youle RJ. Mitochondrial dynamics and apoptosis. Genes Dev. 2008; 22:1577–1590. [PubMed: 18559474]

Sun L, Wang H, Wang Z, He S, Chen S, Liao D, Wang L, Yan J, Liu W, Lei X, et al. Mixed lineage kinase domain-like protein mediates necrosis signaling downstream of RIP3 kinase. Cell. 2012; 148:213–227. [PubMed: 22265413]

Takaki K, Cosma CL, Troll MA, Ramakrishnan L. An in vivo platform for rapid high-throughput antitubercular drug discovery. Cell Rep. 2012; 2:175–184. [PubMed: 22840407]

Thon L, Mohlig H, Mathieu S, Lange A, Bulanova E, Winoto-Morbach S, Schutze S, Bulfone-Paus S, Adam D. Ceramide mediates caspase-independent programmed cell death. Faseb J. 2005; 19:1945–1956. [PubMed: 16319138]

Thwaites GE, Nguyen DB, Nguyen HD, Hoang TQ, Do TT, Nguyen TC, Nguyen QH, Nguyen TT, Nguyen NH, Nguyen TN, et al. Dexamethasone for the treatment of tuberculous meningitis in adolescents and adults. N Engl J Med. 2004; 351:1741–1751. [PubMed: 15496623]

Tiepolo T, Angelin A, Palma E, Sabatelli P, Merlini L, Nicolosi L, Finetti F, Braghetta P, Vuagniaux G, Dumont JM, et al. The cyclophilin inhibitor Debio 025 normalizes mitochondrial function, muscle apoptosis and ultrastructural defects in Col6a1-/- myopathic mice. Br J Pharmacol. 2009; 157:1045–1052. [PubMed: 19519726]

Tobin DM, Roca FJ, Oh SF, McFarland R, Vickery TW, Ray JP, Ko DC, Zou Y, Bang ND, Chau TT, et al. Host genotype-specific therapies can optimize the inflammatory response to mycobacterial infections. Cell. 2012; 148:434–446. [PubMed: 22304914]

Tobin DM, Vary JC Jr, Ray JP, Walsh GS, Dunstan SJ, Bang ND, Hagge DA, Khadge S, King MC, Hawn TR, et al. The lta4h locus modulates susceptibility to mycobacterial infection in zebrafish and humans. Cell. 2010; 140:717–730. [PubMed: 20211140]

Vandenabeele P, Galluzzi L, Vanden Berghe T, Kroemer G. Molecular mechanisms of necroptosis: an ordered cellular explosion. Nature reviews Molecular cell biology. 2010; 11:700–714.

Wallis RS. Reconsidering adjuvant immunotherapy for tuberculosis. Clinical infectious diseases: an official publication of the Infectious Diseases Society of America. 2005; 41:201–208. [PubMed: 15983916]

Wang Z, Jiang H, Chen S, Du F, Wang X. The mitochondrial phosphatase PGAM5 functions at the convergence point of multiple necrotic death pathways. Cell. 2012; 148:228–243. [PubMed: 22265414]

Yang CT, Cambier CJ, Davis JM, Hall CJ, Crosier PS, Ramakrishnan L. Neutrophils exert protection in the early tuberculous granuloma by oxidative killing of mycobacteria phagocytosed from infected macrophages. Cell Host Microbe. 2012; 12:301–312. [PubMed: 22980327]

Zhang DW, Shao J, Lin J, Zhang N, Lu BJ, Lin SC, Dong MQ, Han J. RIP3, an energy metabolism regulator that switches TNF-induced cell death from apoptosis to necrosis. Science. 2009; 325:332–336. [PubMed: 19498109]

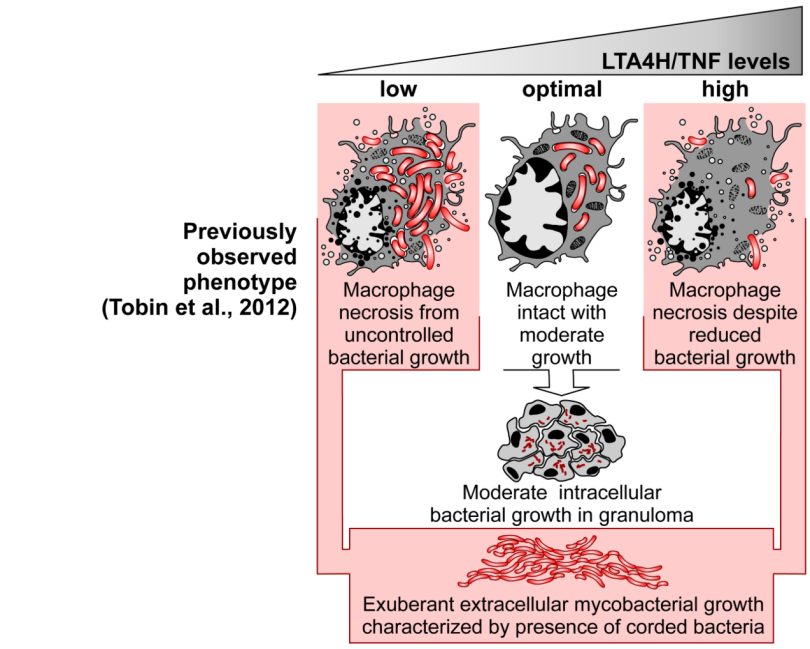

Quantitative Assay

● **Macrophage microbicidal activity** enumerate intracellular bacteria	**low**	**medium**	**high**
● **Infected macrophage lysis** enumerate fluorescent macrophages in *Tg(mpeg1:YFP)* fish, neutral red positive cells, or presence of bacterial cording	**high**	**low**	**high**
● **Susceptibility** — **Early infection:**	**high**	**medium**	**low**
● **Susceptibility** — **Late infection:** assess bacterial burden by Fluorescence Pixel Counts	**high**	**medium**	**high**

Figure 1. Zebrafish susceptibility phenotypes and assays in LTA4H/TNF-low and -high states

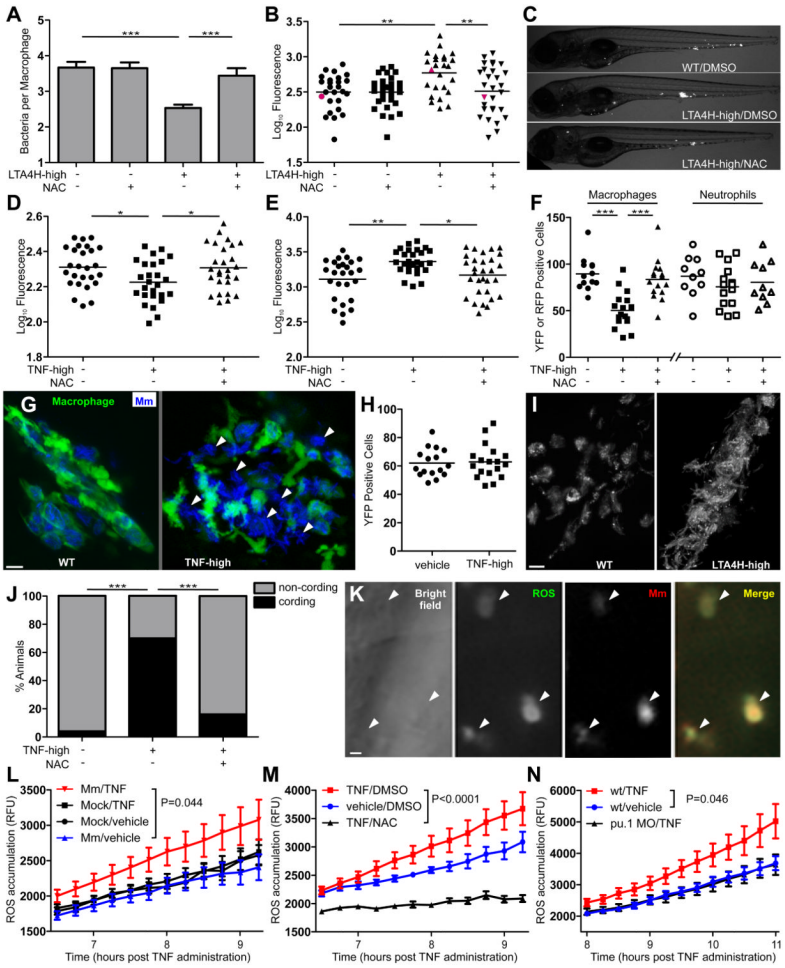

Figure 2. TNF-mediated ROS production kills both mycobacteria and infected macrophages

(A) Mean (±SEM) number of bacteria per infected macrophage in WT and LTA4H-high larvae in presence or absence of 40 μM NAC. ***p < 0.001 (one way ANOVA with Tukey's post-test).

(B) Bacterial burden (FPC) in WT and LTA4H-high siblings in presence or absence of 40 μM NAC. **p < 0.01 (one-way ANOVA with Tukey's post-test). Representative of 2 independent experiments.

(C) Representative fluorescence microscopy images of individual fish in (B) represented by red dots.

(D) FPC of 1 dpi larvae injected with TNF or vehicle with or without 40 μM NAC. *p < 0.05 (one-way ANOVA with Tukey's post-test). Representative of 2 independent experiments.

(E) FPC 3dpi of the same fish in (D). *p < 0.05; **p < 0.01 (one-way ANOVA with Tukey's post-test). Representative of 2 independent experiments.

(F) Number of yellow fluorescent macrophages or red fluorescent neutrophils in 2dpi fish one day after injection with TNF or vehicle in presence or absence of 40 μM NAC. ***p < 0.001 (one-way ANOVA with Tukey's post-test).

(G) Confocal microscopy of granulomas in 3dpi *Tg(mpeg1:YFP)* larvae injected with TNF or vehicle. White arrowheads show extracellular bacteria. Scale bar 10 μm.

(H) Number of yellow fluorescent macrophages in *Tg(mpeg1:YFP)* uninfected fish 1 day post-injection with TNF or vehicle. Difference not significant by Student's t-test. Representative of 2 independent experiments.

(I) Representative fluorescence microscopy images of 4dpi WT and LTA4H-high larva. Scale bar 10 μm.
(J) Percentage of animals in (D) and (E) with cording 4dpi. ***$p < 0.001$ (Fisher's exact test).
(K) Representative fluorescence microscopy images of 1dpi LTA4H-high larvae 6 hours after incubation with CM-H_2DCFDA. Arrowheads point to infected macrophages. Scale bar 10 μm.
(L) Quantification of ROS production as relative fluorescence units (RFU) (±SEM) in WT siblings infected with Mm or mock-infected (See Experimental Procedures) at the indicated time points after injection of TNF or vehicle. (two-way ANOVA). Representative of 2 independent experiments.
(M) Quantification of ROS production as RFU (±SEM) in WT infected siblings at the indicated time points after injection of TNF or vehicle in presence or absence of 40 μM NAC. (two-way ANOVA).
(N) Quantification of ROS production as RFU (±SEM) in infected WT or PU.1 morphant siblings at the indicated time points after injection of TNF or vehicle. (two-way ANOVA). (Also see Figures S1, S2 and S3).

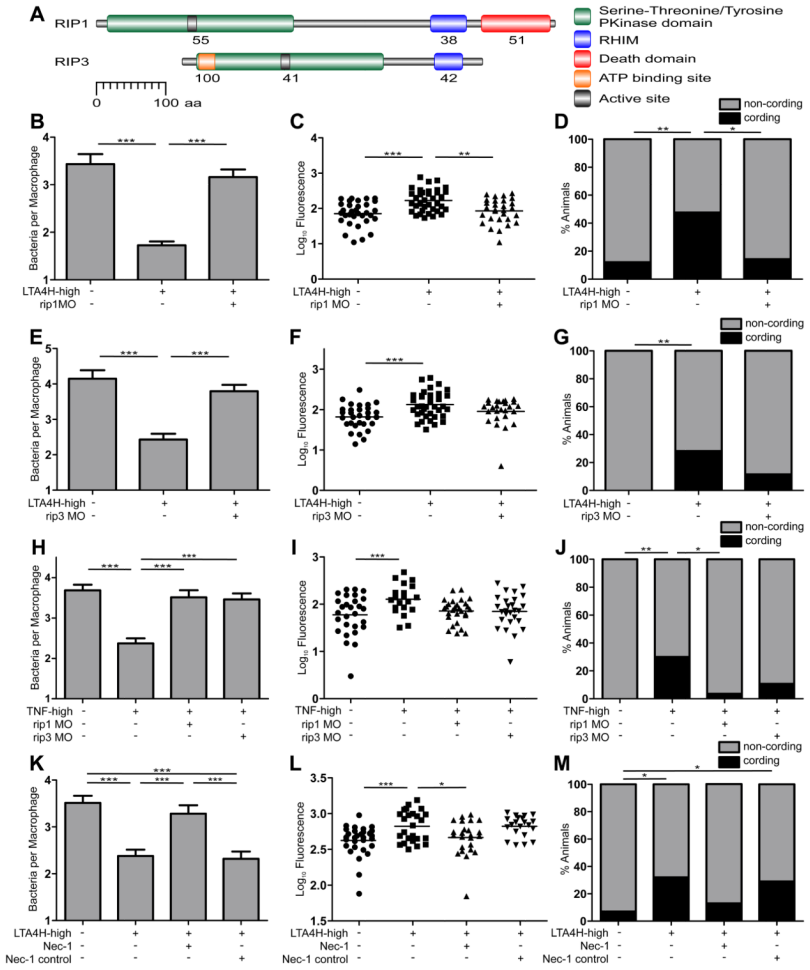

Figure 3. TNF excess mediates necrosis through the RIP1-RIP3 kinase pathway

(A) Zebrafish RIP1 and RIP3 amino acid residue analysis for protein domains. RHIM, RIP homotypic interaction motif; aa, amino acid residue. Numbers indicate percent identity between zebrafish and human domains.

(B) Mean (±SEM) number of bacteria per infected macrophage in WT and RIP1 morphant siblings on LTA4H-high or WT background. ***p < 0.001 (one way ANOVA with Tukey's post-test). Representative of 2 independent experiments.

(C) FPC in WT and RIP1 morphant siblings on LTA4H-high or WT background. **p < 0.01; ***p < 0.001 (one-way ANOVA with Tukey's post-test). Representative of 3 independent experiments.

(D) Percentage of animals in (C) with cording among WT, RIP1 morphants and RIP1 morphants on LTA4H-high background. *p < 0.05; **p < 0.01 (Fisher's exact test).

(E) Mean (±SEM) number of bacteria per infected macrophage in WT and RIP3 morphant siblings on LTA4H-high or WT background. ***p < 0.001 (one way ANOVA with Tukey's post-test). Representative of 2 independent experiments.

(F) FPC in WT and RIP3 morphant siblings on LTA4H-high or WT background. ***p < 0.001 (one-way ANOVA with Tukey's post-test). Representative of 3 independent experiments.

(G) Percentage of animals in (F) with cording among WT, RIP3 morphants and RIP3 morphants on LTA4H-high background. **p < 0.01 (Fisher's exact test).

(H) Mean (±SEM) number of bacteria per infected macrophage in WT and RIP1 or RIP3 morphant larvae injected with TNF or vehicle. ***$p < 0.001$ (one way ANOVA with Tukey's post-test).
(I) FPC in infected WT and RIP1 or RIP3 morphant larvae injected with TNF or vehicle. **$p < 0.01$ (one-way ANOVA with Tukey's post-test).
(J) Percentage of animals in (I) with cording among WT, RIP1 and RIP3 morphants injected with TNF or vehicle. *$p < 0.05$; **$p < 0.01$ (Fisher's exact test).
(K) Mean (±SEM) number of bacteria per infected macrophage in WT and LTA4H-high larvae in presence of 10 μM Necrostatin-1 or 10 μM Necrostatin-1 inactive control. ***$p < 0.001$ (one way ANOVA with Tukey's post-test). Representative of 2 independent experiments.
(L) FPC in WT and LTA4H-high larvae in presence of 10 μM Necrostatin-1 or 10 μM Necrostatin-1 inactive control. *$p < 0.05$; ***$p < 0.001$ (one-way ANOVA with Tukey's post-test). Representative of 2 independent experiments.
(M) Percentage of animals in (L) with cording among WT and LTA4H-high larvae in presence of 10 μM Necrostatin-1 or 10 μM Necrostatin-1 inactive control. *$p < 0.05$ (Fisher's exact test).
(Also see Figures S4 and S5).

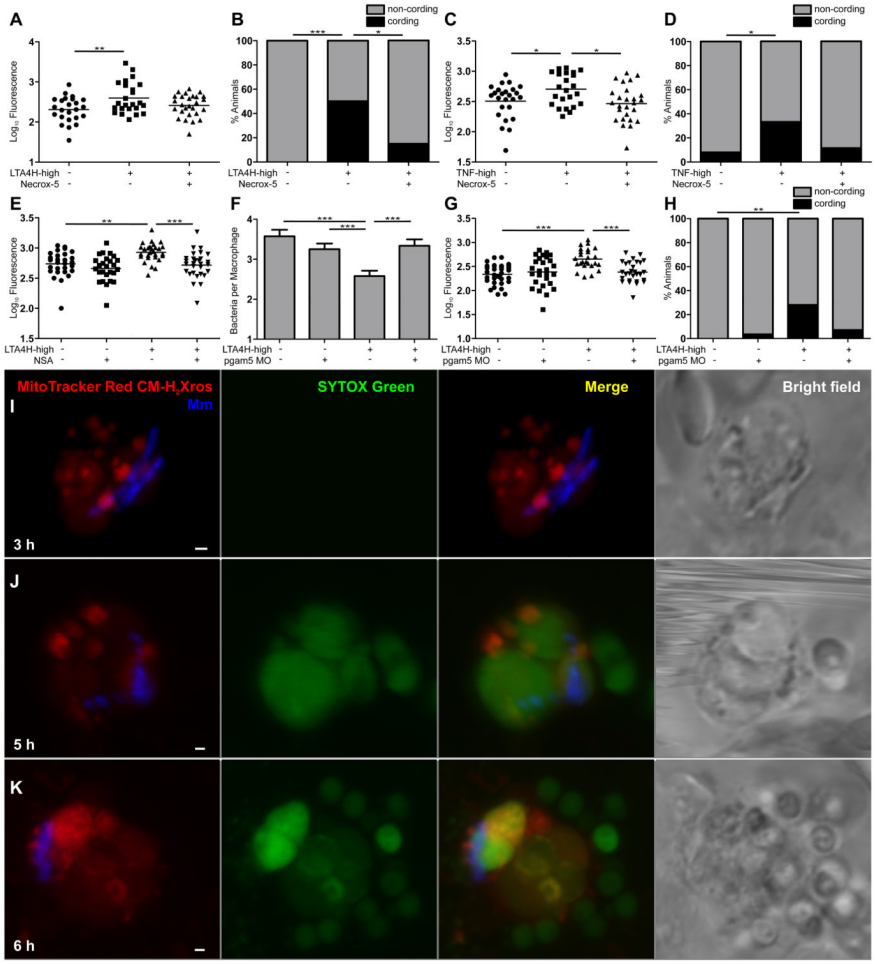

Figure 4. The TNF-RIP1-RIP3 axis mediates necrosis of infected macrophages through mitochondrial ROS production

(A) FPC in WT and LTA4H-high larvae in presence or absence of 10 μM Necrox-5. **p < 0.01 (one-way ANOVA with Tukey's post-test). Representative of 2 independent experiments.

(B) Percentage of animals in (A) with cording among WT and LTA4H-high larvae in presence or absence of 10 μM Necrox-5. *p < 0.05; ***p < 0.001 (Fisher's exact test).

(C) FPC in WT and LTA4H-high larvae injected with TNF or vehicle in presence or absence of 10 μM Necrox-5. *p < 0.05 (one-way ANOVA with Tukey's post-test).

(D) Percentage of animals in (C) with cording among WT and LTA4H-high larvae injected with TNF or vehicle in presence or absence of 10 μM Necrox-5. *p < 0.05 (Fisher's exact test).

(E) FPC in WT and LTA4H-high larvae in presence or absence of 10 μM Necrosulfonamide (NSA). **p < 0.01; ***p < 0.001 (one-way ANOVA with Tukey's post-test). Representative of 3 independent experiments.

(F) Mean (±SEM) number of bacteria per infected macrophage in WT, LTA4H-high and PGAM5 morphant siblings on WT or LTA4H-high background. ***p < 0.001 (one way ANOVA with Tukey's post-test). Representative of 2 independent experiments.

(G) FPC in WT, LTA4H-high and PGAM5 morphant siblings on WT or LTA4H-high background. ***p < 0.001 (one-way ANOVA with Tukey's post-test). Representative of 2 independent experiments.

(H) Percentage of animals in (G) with cording among PGAM5 morphants on WT or LTA4H-high background. **p < 0.01 (Fisher's exact test).
(I-K) Confocal and bright field images of different infected macrophages in 1dpi larvae 3 (I), 5 (J) or 6 (K) hours post-TNF injection. Scale bars 1 μ m.
(Also see Figure S6).

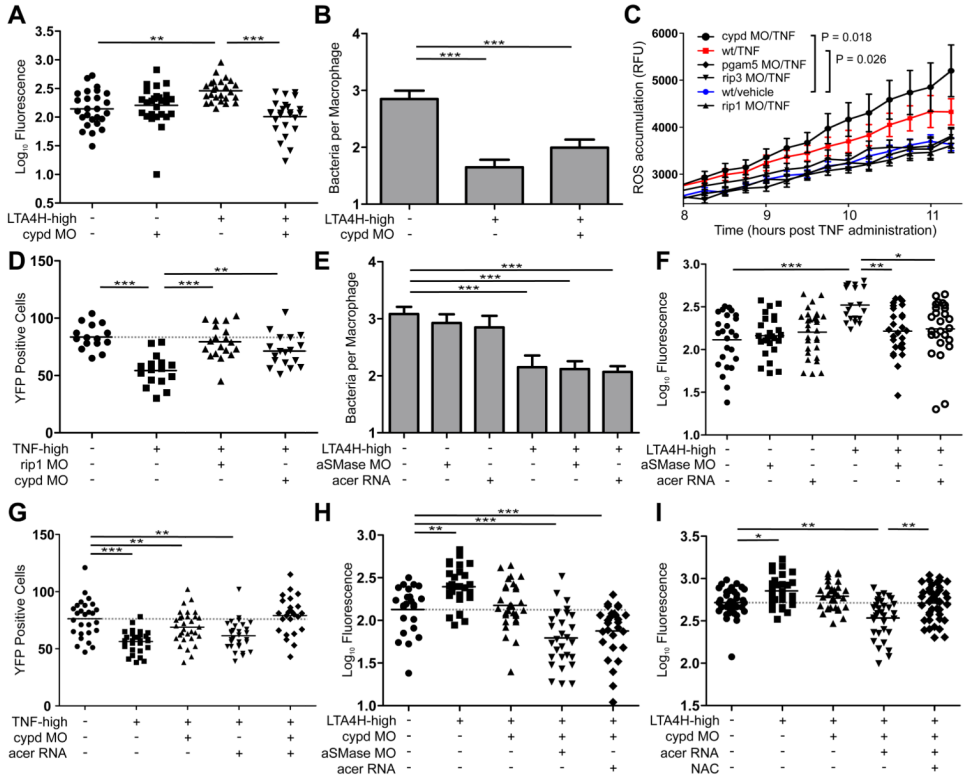

Figure 5. Cyclophilin D and ceramide mediate cell necrosis

(A) FPC in WT or CYPD morphant siblings on WT or LTA4H-high background. **p < 0.01; ***p < 0.001 (one-way ANOVA with Tukey's post-test). Representative of 3 independent experiments.

(B) Mean (±SEM) number of bacteria per infected macrophage in WT, LTA4H-high and CYPD morphants siblings on LTA4H-high background. ***p < 0.001 (one way ANOVA with Tukey's post-test). Representative of 2 independent experiments.

(C) Quantification of ROS production as RFU (±SEM) in infected WT, RIP1, RIP3, PGAM5 and CYPD morphant siblings at indicated time points after TNF or vehicle injection. (two-way ANOVA).

(D) Number of yellow fluorescent macrophages in 2 dpi *Tg(mpeg1:YFP)* RIP1 or CYPD morphant siblings 1 day post-injection with TNF or vehicle. **p < 0.01; ***p < 0.001 (one-way ANOVA with Tukey's post-test). Representative of 2 independent experiments.

(E) Mean (±SEM) number of bacteria per infected macrophage in WT, LTA4H-high and aSMase morphants and acid ceramidase-overexpressing (acer) siblings on WT or LTA4H-high background. ***p < 0.001 (one way ANOVA with Tukey's post-test). Representative of 2 independent experiments.

(F) FPC in WT, LTA4H-high, aSMase morphants and acid ceramidase-overexpressing siblings on WT or LTA4H-high background.*p < 0.05; **p < 0.01; ***p < 0.001 (one-way ANOVA with Tukey's post-test). Representative of 2 independent experiments.

(G) Number of yellow fluorescent macrophages in 2 dpi *Tg(mpeg1:YFP)* CYPD morphants and ceramidase-overexpressing siblings 1 day post-injection with TNF or vehicle. **p < 0.01; ***p < 0.001 (one-way ANOVA with Tukey's post-test). Dashed line, control group mean.

(H) FPC in WT, LTA4H-high, CYPD morphants, double CYPD/aSMase morphants and CYPD morphants-overexpressing simultaneously acid ceramidase on LTA4H-high

background.*p < 0.05; **p < 0.01; ***p < 0.001 (one-way ANOVA with Tukey's post-test). Representative of 2 independent experiments. Dashed line, control group mean.
(I) FPC in WT, LTA4H-high, CYPD morphants and CYPD morphants-overexpressing simultaneously acid ceramidase on LTA4H-high background in presence or absence of 40 μM NAC.*p < 0.05; **p < 0.01; ***p < 0.001 (one-way ANOVA with Tukey's post-test). Representative of 2 independent experiments. Dashed line, control group mean.

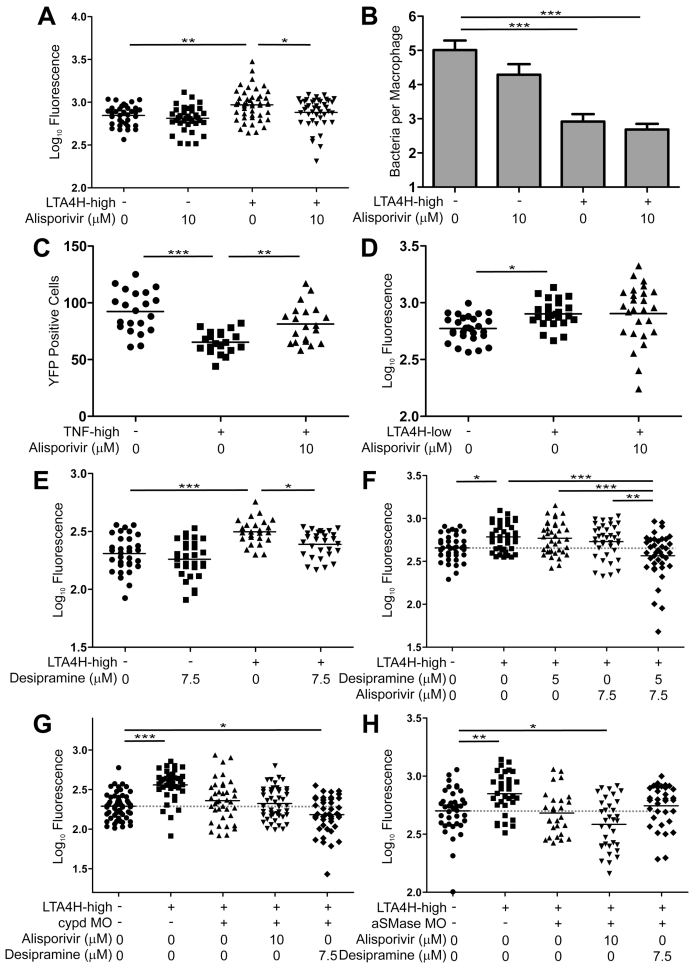

Figure 6. Drugs blocking cyclophilin D- and ceramide-mediated necrosis synergize as host-targeting therapies for high-TNF mediated TB

(A) FPC in WT and LTA4H-high larvae treated with Alisporivir or left untreated. *p < 0.05; **p < 0.01 (one-way ANOVA with Tukey's post-test). Representative of 3 independent experiments.

(B) Mean (±SEM) number of bacteria per infected macrophage in WT and LTA4H-high siblings in presence or absence of Alisporivir. ***p < 0.001 (one way ANOVA with Tukey's post-test). Representative of 2 independent experiments.

(C) FPC in WT siblings injected or not with TNF in presence or absence of Alisporivir. **p < 0.01; ***p < 0.001 (one-way ANOVA with Tukey's post-test).

(D) FPC in WT and LTA4H-low siblings in presence or absence of Alisporivir. *p < 0.05 (oneway ANOVA with Tukey's post-test).

(E) FPC in WT and LTA4H-high larvae in presence or absence of Desipramine. *p < 0.05; ***p < 0.001 (one-way ANOVA with Tukey's post-test). Representative of 3 independent experiments.

(F) FPC in WT and LTA4H-high larvae in presence or absence of Desipramine, Alisporivir or the combination of both. *p < 0.05; **p < 0.01; ***p < 0.001 (one-way ANOVA with Tukey's post-test). Representative of 2 independent experiments. Dashed line, control group mean.

(G) FPC in WT, LTA4H-high and LTA4H-high/CYPD morphant larvae treated with Alisporivir, Desipramine or left untreated. ***p < 0.001 (one-way ANOVA with Dunnett's post-test). Representative of 2 independent experiments. Dashed line, control group mean.

(H) FPC in WT, LTA4H-high and LTA4H-high/aSMase morphant larvae treated with Alisporivir, Desipramine or left untreated. *$p < 0.05$; **$p < 0.01$ (one-way ANOVA with Dunnett's post-test). Dashed line, control group mean.

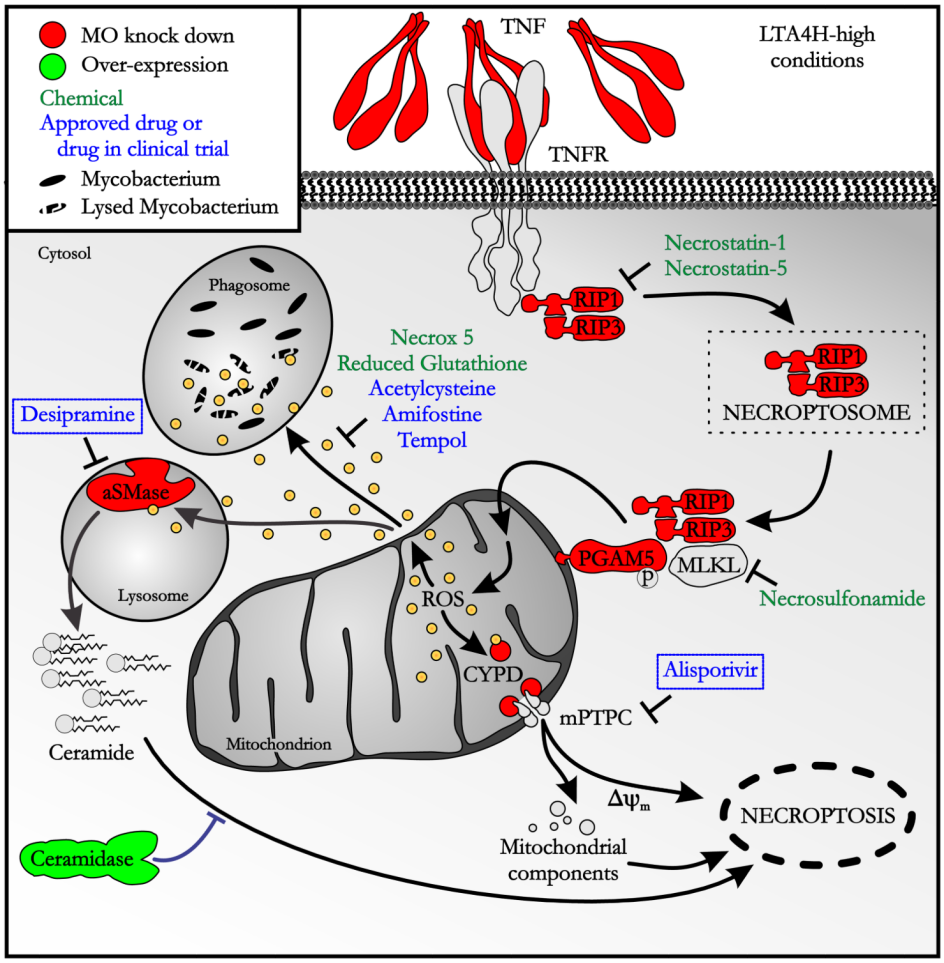

Figure 7. TNF-dependent programmed necrosis pathways showing genetic and chemical interventions used in this study

Δψm, dissipation of mitochondrial membrane potential (also see Table S3)